Korean J. Chem. Eng., **31**(11), 2057-2069 (2014)
DOI: 10.1007/s11814-014-0176-2

pISSN: 0256-1115
eISSN: 1975-7220

Equilibrium arsenic adsorption onto metallic oxides : Isotherm models, error analysis and removal mechanism

Esra Bilgin Simsek*,† and Ulker Beker**

*Chemical and Process Engineering Department, Yalova University, Yalova 77100, Turkey
**Chemical Engineering Department, Yldz Technical University, Istanbul 34220, Turkey
(*Received 12 April 2014 • accepted 24 June 2014*)

Abstract−Arsenic adsorption properties of mono- (Fe or Al) and binary (Fe-Al) metal oxides supported on natural zeolite were investigated at three levels of temperature (298, 318 and 338 K). All data obtained from equilibrium experiments were analyzed by Freundlich, Langmuir, Dubinin-Radushkevich, Sips, Toth and Redlich-Peterson isotherms, and error functions were used to predict the best fitting model. The error analysis demonstrated that the As(V) adsorption processes were best described by the Dubinin-Raduskevich model with the lowest sum of normalized error values. According to results, the presence of iron and aluminum oxides in the zeolite network improved the As(V) adsorption capacity of the raw zeolite (ZNa). The X-ray photoelectron spectroscopy (XPS) analyses of ZNa-Fe and ZNa-AlFe samples suggested that the redox reactions are the postulated mechanisms for the adsorption onto them while the adsorption process is followed by surface complexation reactions for ZNa-Al.

Keywords: Adsorption, Arsenic, Isotherm, Metal Oxide, Error Analysis, XPS

INTRODUCTION

In the past decades, the occurrence of arsenic in natural waters, mainly in groundwater, has been a serious environmental problem all over the world due to its high toxicology. Acute and chronic arsenic exposure via drinking water has been reported in countries like Argentina, Bangladesh, Mexico, India, Thailand, and Taiwan, where a large proportion of groundwater is contaminated with arsenic up to 2,000 μg L^{-1} [1]. Long-term exposure to arsenic via water sources could cause vascular and skin diseases as well as lung, bladder and kidney cancer. To prevent the health problems associated with As in drinking water, the US EPA (the Environmental Protection Agency of the United States of America) has decreased the acceptable maximum contaminant level (MCL) of As from 50 to 10 μg L^{-1}. Thus, effective treatment methods for arsenic removal from water sources must be taken in order to meet the standard. Especially, developing countries have to consider low-cost and simple removal techniques [1]. Several techniques of arsenic removal, such as precipitation, ion-exchange, adsorption, reverse osmosis and ultrafiltration, are already available [2]. Adsorption has also emerged as a more popular alternative technique due to its simplicity, potential to offer a sludge-free operation and availability of using many kinds of adsorbents [3,4].

More recently, zeolites have received increasing attention in the context of pollution control, emerging as standard components of wastewater treatment [5]. Since the application of zeolites is simple and as they require mild operating conditions, they have been used for the selective separation of toxic elements from aqueous solutions [6]. However, arsenic is found as anionic species like trivalent arsenite $(AsO_2)^-$ or less toxic pentavalent arsenate $(HAsO_4)^{2-}$ which cannot be exchangeable by the cations from zeolite. The possibility of chemical modification of zeolite surface with metallic oxides or surfactants allows zeolites to be effective adsorbents for anionic species [5-10]. Several papers have focused on the strong adsorption affinity of arsenic to Fe or Al oxides/hydroxides forming very stable As-Fe/Al complexes. Doušová et al. [11] studied As(V) adsorption onto three adsorbents, metakaoline, clinoptilolite-rich tuff and synthetic zeolite, in both pure and iron oxide treated forms. They found the adsorption capacity increased significantly for iron oxide treated samples when compared with untreated ones (from about 0.5 to >20.0 mg g^{-1}). Macedo-Miranda and Olguin [9] modified the Mexican clinoptilolite-heulandite rich tuffs with iron oxides, and they calculated the Langmuir As(V) sorption capacity as 53.6 μg g^{-1} (at pH 6). Jiménez-Cedillo et al. [5] investigated the As(V) and As(III) sorption properties of iron and iron-manganese-modified clinoptilolite-rich tuffs, and they suggested that the removal of As(III) and As(V) by the zeolitic materials might be influenced by the nature of the arsenic chemical species, the origin of the natural zeolite and the textural characteristics of the modified material. Ramesh et al. [12] studied the As(III), As(V) and dimethylarsenate (DMA) adsorption onto polymeric Al/Fe modified montmorillonite. They found that the DMA adsorption capacity of the adsorbent was higher compared to the literature values, and the adsorbent could be used in more than five cycles of sorption-desorption without any significant change of adsorption capacity.

The magnetic forms of iron oxides have also been used efficiently for arsenic removal and, after adsorption, these sorbents can be separated from solution by using an external magnetic field. Yavuz et al. [13] proposed the use of magnetite particles for arsenic decontamination of water based on their magnetic properties. They reported that, as the arsenic species are negatively charged in the acidic pH range, electrostatic attraction occurs between magnetite-maghemite nanoparticles and arsenic anions. Liu et al. [3] showed that the mag-

†To whom correspondence should be addressed.
E-mail: esrabilgin622@gmail.com

netite iron oxide had a higher adsorption capacity to As(V) (3.6 mg g^{-1}) than that to As(III). The optimal pH range for As(III) adsorption was determined as between 6-9.4, while the adsorption was better under the acidic conditions for As(V). Furthermore, a number of papers have reported about the mixed form of the iron and aluminum oxides showing better efficiency than many of the single metal oxides [14-18]. Therefore, the present study focused on the As(V) adsorption onto mono- (Fe or Al) and binary (Fe/Al) oxides supported on natural zeolite. Adsorption characteristics were investigated using the isotherm models in a series of batch experiments. The magnetization measurements and X-ray photoelectron spectroscopy (XPS) analyses were used to elucidate the magnetization character and arsenic adsorption mechanism, respectively.

MATERIALS AND METHODS

1. Chemicals and Reagents

All the chemicals/reagents used in this work were of analytical reagent grade. The ferrous chloride ($FeCl_2 \cdot 4H_2O$), ferric chloride ($FeCl_3 \cdot 6H_2O$), anhydrous aluminum chloride ($AlCl_3$) and sodium hydroxide (NaOH) were purchased from Sigma-Aldrich. The As(V) stock solutions were prepared by dissolving $Na_2HAsO_4 \cdot 7H_2O$ in deionized water. The natural zeolite was obtained from Gördes-Manisa deposit, produced by Rota Mining Company, Turkey. The average chemical composition of zeolite [chemical formula: $(Ca,K_2,Na_2,Mg)_4 Al_8Si_{40}O_{96} \cdot 24H_2O$] is reported as SiO_2 - 65-72% and Al_2O_3 - 10-12% (wt).

2. Preparation of Mono and Binary Metal Oxides

The previous work [4] indicated that the pretreated zeolites exhibited low or no adsorption efficiency for As(V). However, major increases in As(V) adsorption capacities were observed for the metal oxide coated zeolites. While As(V) adsorption capacity of pretreated zeolite was 0.026 mg g^{-1} it increased to 2.00-5.0 mg g^{-1} after modification with iron and aluminum oxides. For that reason, the present study aimed to explore arsenic adsorption onto mono and binary oxides doped natural zeolites in detail. Briefly, the raw clinoptilolite was treated with 2 mol L^{-1} NaCl solution (coded as ZNa). Then, a definite amount of ZNa was added to 200 mL of Fe(II) solution, and the resulting suspension was stirred while adding 5 mol L^{-1} NaOH, allowing iron oxide particles to precipitate onto its surface. After stirring for 1 h, the sample was washed with deionized water and dried overnight at 338 K (designated as ZNa-Fe). Aluminum oxide coated zeolite was prepared according to the same procedure described above using Al^{3+} solution (coded as ZNa-Al). Binary metal oxide (Fe&Al) coated zeolite was prepared by using a mixture of $AlCl_3$ and $FeCl_3$ solutions and NaOH was added dropwise to the suspension till pH reached 10-11. The resultant sample was dried at 338 K and denoted as ZNa-AlFe.

3. Characterization

Magnetic properties of iron oxide coated zeolites (ZNa-Fe and ZNa-AlFe) were characterized by Quantum Design Physical Property Measurement System (PPMS-9T) at ambient temperature. Exhausted adsorbents were analyzed by using X-ray photoelectron spectroscopy (VSW, Vacuum System Workshop Ltd, England equipped with PHOIBOS 100 spectrometer).

4. Adsorption Isotherms

An adsorption isotherm is the basic source of information about the adsorption process [19]. The isotherm models can be based on models with two, three or more parameters [20]. Due to the limited application of two-parameter models, there is a growing interest in the derivation of isotherm models [21]. In the present study, the relationship between adsorbed As(V) and the concentrations at equilibrium was described by two- and three-parameter isotherm models: Freundlich, Langmuir, Dubinin-Radushkevich, Redlich-Peterson, Sips, and Toth using STATISTICA (Ver. 8.0, StatSoft Inc., USA) software package.

4-1. Langmuir Model

The Langmuir model assumes homogeneous adsorption in which each molecule has equal enthalpy and sorption activation energy [22]. The model is expressed as:

$$q_e = \frac{Q \cdot b \cdot C_e}{1 + b \cdot C_e} \quad (1)$$

where q_e is the adsorbed amount at equilibrium (mg g^{-1}), C_e is the equilibrium concentration of the adsorbate (mg L^{-1}), Q is the Langmuir monolayer sorption capacity (mg g^{-1}) and b is the Langmuir equilibrium constant (L mg^{-1}) related to the energy of adsorption and affinity of the adsorbent. Webber and Chakkravorti [23] defined a dimensionless constant, R_L, which describes the type of isotherm and is represented as:

$$R_L = 1/(1 + b \cdot C_i) \quad (2)$$

where C_i is the initial adsorbate concentration (mg L^{-1}). The magnitude of R_L determines the adsorption nature to be either unfavorable ($R_L > 1$), linear ($R_L = 1$), favorable ($0 < R_L < 1$) or irreversible ($R_L = 0$).

4-2. Freundlich Model

The model is based on multilayer adsorption, with non-uniform distribution of adsorption heats and affinities over the heterogeneous surface. The model is not restricted to the formation of monolayer as Langmuir theory [20]. The model is expressed by the following equation:

$$q_e = K_F \cdot C_e^{1/n} \quad (3)$$

where K_F and n are indicative isotherm parameters of adsorption capacity (mg g^{-1}) and intensity, respectively. The 1/n value is a sign of surface heterogeneity and ranges between 0 and 1. The adsorption becomes more heterogeneous as it is closer to zero [24,25].

4-3. Dubinin-Radushkevich (D-R) Isotherm Model

The D-R model is based on the assumption of multilayer character of the adsorbent surface and is generally applied to distinguish the physical and chemical adsorption mechanisms [26]. The isotherm is expressed by [27]:

$$q_e = q_m \cdot \exp(-\beta \cdot \varepsilon^2) \quad (4)$$

$$\varepsilon = R \cdot \ln(1 + 1/C_e) \quad (5)$$

where R indicates gas constant (8.314 J mol^{-1} K^{-1}), T and C_e are absolute temperature (K) and equilibrium concentration (mg L^{-1}), respectively.

4-4. Redlich-Peterson Model

Redlich-Peterson model is an empirical hybrid isotherm combining Langmuir and Freundlich isotherms. The isotherm theory does not assume ideal monolayer adsorption [28]. The empirical equation is:

$$q_e = \frac{K_{RP} \cdot C_e}{(1 + \alpha_{RP} \cdot C_e^{\beta_{RP}})} \quad (6)$$

α_{RP} and K_{RP} are the Redlich-Peterson isotherm constants, and β_{RP} is the exponent which ranges between 0 and 1. The model fits the Freundlich isotherm at high concentrations ($\beta_{RP} \approx 0$), while it approaches the ideal Langmuir condition at low concentrations ($\beta_{RP} \approx 1$) [20].

4-5. Toth Model

Toth isotherm is the modified form of Langmuir equation by minimizing the errors between experimental and theoretical data of adsorption [29]. The model equation is derived from the potential theory and suited to multilayer adsorption similar to BET isotherms, which is a special type of Langmuir isotherm [30]. The Toth equation is given as:

$$q_e = \frac{q_{mT} \cdot C_e}{\left(\frac{1}{K_T} + C_e^{mT}\right)^{1/mT}} \quad (7)$$

where q_{mT} is the Toth maximum adsorption capacity (mg g^{-1}), K_T and m_T are the Toth equilibrium constant and Toth model exponent, respectively.

4-6. Sips Model

Sips isotherm is a combination of Langmuir and Freundlich models predicting non-uniform surfaces on adsorption system [31]. Mathematically, it can be described as follows:

$$q_e = \frac{q_{mS} \cdot K_S \cdot C_e^{ms}}{(1 + K_S \cdot C_e^{ms})} \quad (8)$$

where q_{mS} is the indicator of Sips maximum adsorption capacity (mg g^{-1}), K_S and m_s are the Sips equilibrium constant (L mg^{-1}) and model exponent, respectively. The model reduces to the Freundlich isotherm at low concentrations, while at high concentrations it assumes a monolayer adsorption characteristic of the Langmuir isotherm [32].

Adsorption isotherm studies were performed by varying amounts of adsorbent (2-200 mg) in 50 mL conical flasks with 5.0 mg L^{-1} As(V) concentration at different temperatures (298, 318 and 338 K). The initial pH values of the solutions were adjusted to 3.0 (ZNa-Fe) and 5.0 (ZNa-Al, ZNa-AlFe) according to the previous study [4]. During the adsorption experiments, pH of the solutions was kept constant by using diluted HCl or NaOH twice in a day. The arsenic was determined by atomic absorption spectrophotometer (Analytic Jena ContrAA 700 TR). The analyses were conducted at a wavelength of 193.7 nm by a graphite furnace system using Pd/$Mg(NO_3)_2$ as a matrix modifier. Dilution was made with 2% HNO_3 solution and samples were reanalyzed in case the relative standard deviation exceeded 5%. The As(V) adsorption capacity (q_e) was calculated from the following equation:

$$q_e = \frac{(C_i - C_e) \times V}{m} \quad (9)$$

where q_e is the adsorption capacity (mg g^{-1}), C_i is the initial concentration of arsenate (mg L^{-1}), V is the solution volume (L) and m is the adsorbent dosage (g).

5. Error Analysis

In adsorption isotherm studies, an optimization procedure requires error functions in order to determine the fitness of applied model to the experimental data. For that reason, the coefficient

$$R^2 = \frac{\sum (q_{cal} - q_{a\,exp})^2}{\sum (q_{cal} - q_{a\,exp})^2 + (q_{cal} - q_{exp})^2} \quad (10)$$

of determination (R^2) values were calculated by using Eq. (10):

Moreover, Chi-square values (χ^2) were calculated to estimate the isotherm models:

$$\chi^2 = \sum \left[\frac{(q_{exp} - q_{cal})^2}{q_{cal}} \right] \quad (11)$$

where q_{cal} and q_{exp} refer to the theoretical and experimental capacities (mg g^{-1}), respectively, and $q_{a\,exp}$ is the average experimental capacity. However, interpreting of R^2 and χ^2 values is insufficient to evaluate the goodness of fit and compare the isotherm models. El-Khaiary and Malash [33] reported that in the statistically analyzing process of the experimental data, the adsorption literature contains errors which render the results unreliable. They also highlighted the most obvious issues with R^2. Therefore, in the present study, five error functions were calculated across the studied range using the Solver add-in with Microsoft's spreadsheet, Microsoft Excel. In each case, the isotherm parameters were determined by minimizing the respective error function. The error functions studied were as follows:

5-1. The Sum of the Squares of the Errors (ERRSQ)

This error function is widely used and the magnitude of function indicates the goodness of the applied model. However, it has one major drawback that the squares of errors increases by increasing concentration and so the model provides better fit to the experimental data [34].

$$ERRSQ = \sum_{i=1}^{p} (q_{exp} - q_{cal})_i^2 \quad (12)$$

5-2. The Hybrid Fractional Error Function (HYBRID)

Porter et al. [35] developed HYBRID error function to improve the fit of the ERRSQ function at low concentrations.

$$HYBRID = \frac{100}{n-p} \sum_{i=1}^{p} \left[\frac{(q_{exp} - q_{cal})^2}{q_{exp}} \right]_i \quad (13)$$

Here, n is the number of data points and p is the number of parameters of the isotherm equation [36].

5-3. Marquardt's Percent Standard Deviation (MPSD)

Marquardt's equation is similar to a geometric mean error distribution which is modified to allow for the number of degrees of freedom in the system.

$$MPSD = 100 \left[\sqrt{\frac{1}{n-p} \sum_{i=1}^{p} \left(\frac{q_{exp} - q_{cal}}{q_{exp}} \right)_i^2} \right] \quad (14)$$

5-4. The Sum of the Absolute Errors (EABS)

The isotherm model parameters determined by using the EABS function provide a better fit as the magnitudes of the errors increase [34].

$$EABS = \sum_{i=1}^{p} |q_{exp} - q_{cal}|_i \quad (15)$$

5-5. The Average Relative Error (ARE)

This error function attempts to minimize the fractional error distribution across the entire concentration range [37].

$$ARE = \frac{100}{p}\sum_{i=1}^{p}\left(\frac{|q_{exp} - q_{cal}|}{q_{exp}}\right)_i \quad (16)$$

Each of the above error functions produces a different set of isotherm parameters. Thus, to identify which set is an optimum parameter, the 'sum of the normalized errors' (SNE) for each parameter set was determined [30]. Each error function for each set of isotherm constants was divided by the maximum error function from that set to determine the normalized errors. According to this method, the error function with the minimum SNE value can be accepted to give the closest fit.

RESULTS AND DISCUSSION

1. Characterization

Fig. 1 presents the magnetization curves obtained for iron oxide modified zeolites. The saturation magnetization (M_s) value of ZNa-Fe was 0.39 emu g^{-1} at ambient temperature, while that of for ZNa-AlFe was 0.0005 emu g^{-1}. Furthermore, ZNa-Fe has a hysteresis indicating super-paramagnetism while no evidence of magnetism was seen for ZNa-AlFe sample. ZNa-Fe particles were attracted toward the magnet while ZNa-AlFe was not attracted. Therefore, the magnetic ZNa-Fe can be used efficiently for As(V) removal and, after adsorption, this sorbent can be easily separated from solution by using an external magnetic field.

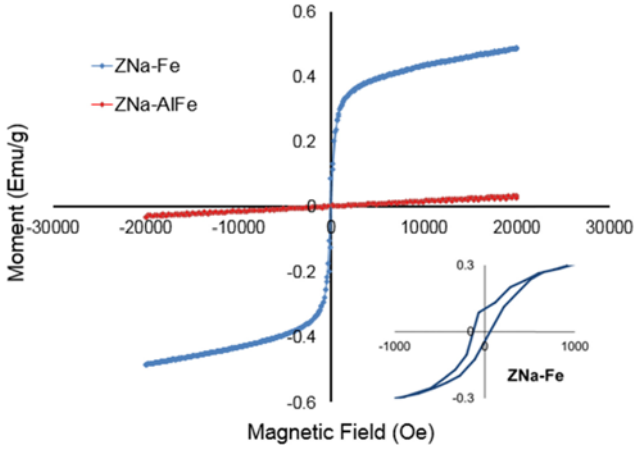

Fig. 1. Magnetization curves of iron oxide modified zeolites.

2. Isotherm Models and Error Analysis

The plots of Freundlich, Langmuir, D-R, Redlich-Peterson, Sips, and Toth isotherm models for As(V) adsorption onto raw and modified zeolites are presented in Figs. 2-5. The calculated values of ZNa were too low due to the low adsorption capacity and the applied models were not described well. The illustrated isotherm curves of ZNa (Fig. 2) indicated that the As(V) adsorption was fitted to Type-III isotherm suggesting weak adsorbate–adsorbent interactions.

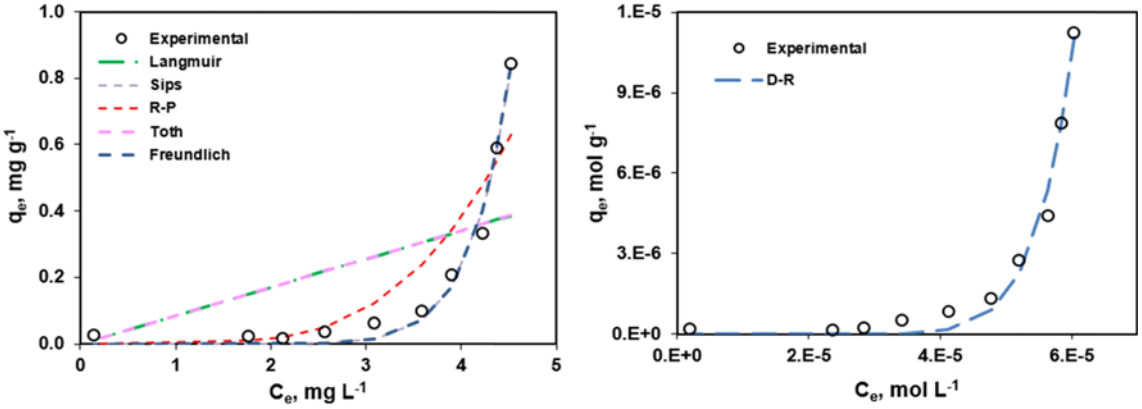

Fig. 2. Non-linear isotherms of ZNa (pH 5, C_i: 5 mg L^{-1}, T: 298 K).

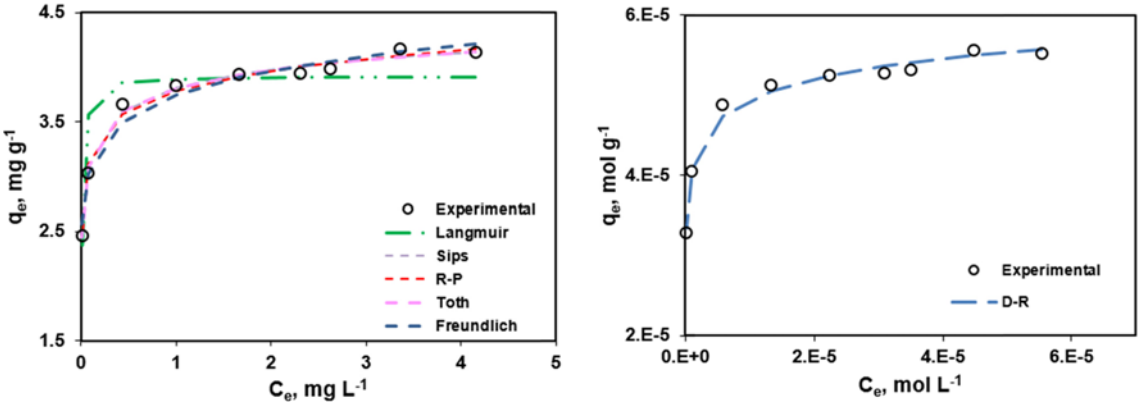

Fig. 3. Non-linear isotherms of ZNa-Fe (pH 3, C_i: 5 mg L^{-1}, T: 298 K).

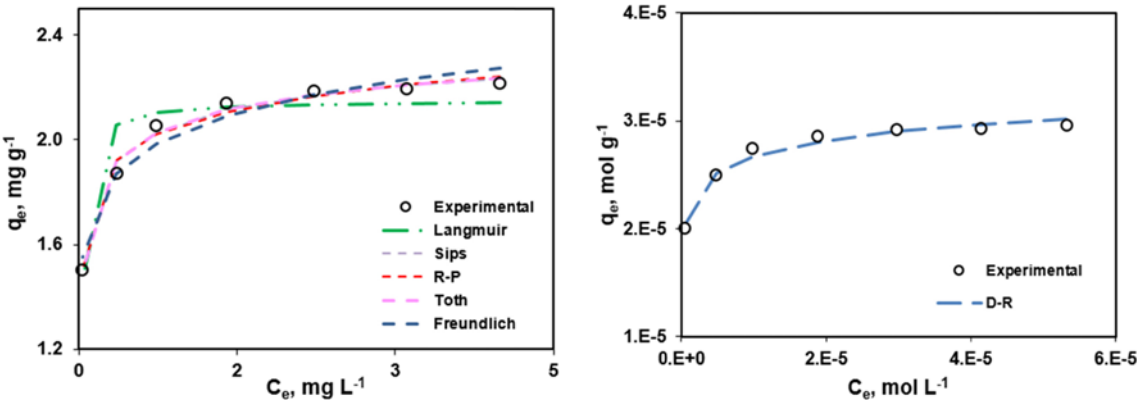

Fig. 4. Non-linear isotherms of ZNa-Al (pH 5, C_i: 5 mg L^{-1}, T: 298 K).

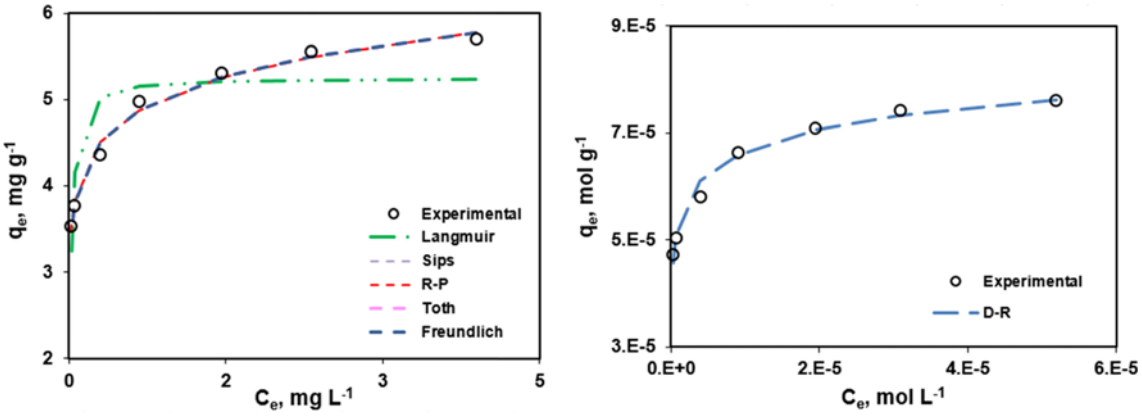

Fig. 5. Non-linear isotherms of ZNa-AlFe (pH 5, C_i: 5 mg L^{-1}, T: 298 K).

Taking R^2 (≥0.990) and χ^2 (≤0.004) values into account, the most appropriate isotherms were found as D-R and Toth models for the ZNa-Fe sample. The R-P and Sips equations also seem suitable due to the low χ^2 values (Table 1). The maximum adsorption capacities calculated using the Langmuir model were lower than those of Toth, Sips, Redlich-Peterson models. It shows that the As(V) adsorption onto the ZNa-Fe adsorbent did not occur on the homogeneous surface.

The adsorption on ZNa-Al was suited to the Dubinin-Raduskevich and Redlich-Peterson isotherms (Fig. 4), which correctly simulates to the experimental data, while the Langmuir model showed the highest error values. As seen in Table 2, among the two-parameter isotherms, the D-R isotherm model describes the adsorption system well (SNE_{ERRSQ}: 1.345; SNE_{HYBRID}: 0.363) and the equilibrium data were found in good agreement with Sips isotherm model (SNE_{HYBRID}: 3.986). Moreover, the calculated values of Sips maximum adsorption capacity, model exponent and equilibrium constant were found to be 2.62 mg g^{-1}, 3.71 (L mg^{-1}) and 0.30, respectively. The model exponents of Sips (m_S) for ZNa-Fe, ZNa-Al and ZNa-AlFe were found closer to zero than unity (ranging between 0.05 and 0.2). This supports the fact that As(V) adsorption on modified zeolites fitted more the Freundlich theory than of Langmuir [30,38].

The obtained results (Table 3) for ZNa-AlFe showed that the best-fitted adsorption isotherm models were in the order of: D-R>Sips> Redlich-Peterson>Toth>Freundlich>Langmuir, on the basis of high R^2 and lower χ^2 values. The HYBRID and ERRSQ parameter sets produced the best fit to the D-R model by giving the lowest SNE values (SNE_{HYBRID}=0.231; SNE_{ERRSQ}=1.226). The D-R model adsorption capacities for ZNa-Fe, ZNa-Al and ZNa-AlFe samples were calculated as 4.15, 2.26 and 5.94 mg g^{-1}, respectively. Among the three-parameter models, the Sips isotherm describes with satisfaction the equilibrium data due to the lower SNE value (SNE_{HYBRID}=4.221).

3. Isosteric Heat of Adsorption

The heat of adsorption, which was determined at constant amount of adsorbate adsorbed is defined as the isosteric heat of adsorption (ΔH_x, kJ mol^{-1}), is one of the basic requirements for the characterization and optimization of adsorption processes [39]. The isosteric heats of adsorption are the key thermodynamic variables for the design of separation processes [40]. The isosteric heat of adsorption is calculated using the following equation, which is derived from the Clausius-Clapeyron equation.

$$\frac{d(\ln C_e)}{dT} = -\frac{\Delta H_x}{RT^2} \quad (17)$$

For this purpose, the plots of ln C_e versus 1/T were derived for different amounts of adsorbed As(V) at different temperatures (298, 318, 338 K). The plots of ln C_e versus 1/T were found to be linear (Fig. 6), and the values of ΔH_X were found from the slopes of these isosters. The ΔH_X values as a function of surface loading are shown in Fig. 7. The isosteric heat of adsorption increases with increasing

Table 1. Non-linear isotherm parameters with error analysis of ZNa-Fe sample

	LTFM	ERRSQ	HYBRID	MPSD	ARE	EABS		LTFM	ERRSQ	HYBRID	MPSD	ARE	EABS
Langmuir							***Freundlich***						
b (L mg^{-1})	167.322	138.097	147.153	147.153	164.901	164.661	K_f (mg g^{-1})	3.745	3.745	3.743	3.743	3.765	3.765
Q (mg g^{-1})	3.866	3.917	3.892	3.892	3.954	3.956	n	11.724	12.170	11.920	11.920	11.944	11.945
ERRSQ		0.496	0.502	0.502	0.547	0.548	**ERRSQ**		0.060	0.060	0.061	0.064	0.064
HYBRID		2.187	2.163	2.163	2.415	2.424	**HYBRID**		0.248	0.248	0.244	0.260	0.260
MPSD		14.78	14.707	14.70	15.54	15.570	**MPSD**		4.987	4.987	4.941	5.102	5.103
ARE		5.317	5.3056	5.305	4.552	4.552	**ARE**		1.954	1.954	1.963	1.909	1.909
EABS		1.618	1.646	1.646	1.425	1.424	**EABS**		0.620	0.620	0.631	0.610	0.610
SNE		4.739	4.749	4.749	4.713	4.721	**SNE**		4.841	4.841	4.850	4.938	4.939
R^2:	0.85	χ^2: 0.141					R^2:	0.989	χ^2: 0.018				
D-R							***Sips***						
q_m (mol·g^{-1})	7.7E-05	7.6E-05	7.6E-05	7.6E-05	7.6E-05	7.6E-05	q_m (mg g^{-1})		5.1878	5.2373	5.2373	5.1829	5.1862
β	5.4E-10	5.3E-10	5.3E-10	5.3E-10	5.3E-10	5.3E-10	K_s (L mg^{-1})		2.772	2.6701	2.670	2.786	2.781
ERRSQ		7.22E-10	5.37E-12	5.37E-12	5.37E-12	5.37E-12	m_s		0.246	0.241	0.241	0.244	0.244
HYBRID		1.55E-06	1.55E-06	0.000337	0.000337	0.000337	**ERRSQ**		0.019	0.019	0.019	0.020	0.020
MPSD		0.012	0.012	0.183	0.1834	0.1834	**HYBRID**		0.087	0.087	0.087	0.089	0.089
ARE		1.381	1.381	16.458	16.458	16.458	**MPSD**		2.959	2.956	2.956	2.993	2.994
EABS		6.06E-06	6.06E-06	5.9E-05	5.9E-05	5.9E-05	**ARE**		1.047	1.038	1.038	1.001	1.000
SNE		**1.2593**	**0.2667**	4.0074	4.0074	4.0074	**EABS**		0.346	0.345	0.345	0.336	0.336
R^2:	0.998	χ^2: 1.1E-07					**SNE**		4.947	4.936	4.936	4.928	4.927
							R^2:	0.992	χ^2: 0.005				
R-P							***Toth***						
K_{RP} (L g^{-1})		2065.925	2205.459	2205.294	2013.995	2059.285	q_m (mg g^{-1})		5.638	5.732	5.732	5.633	5.626
a_{RP} (L mg^{-1})		545.316	582.719	582.675	532.203	545.760	K		14.272	14.136	14.136	14.449	14.462
β_{RP}		0.932	0.931	0.931	0.934	0.935	M_t		0.172	0.166	0.166	0.171	0.171
ERRSQ		0.029	0.029	0.029	0.031	0.033	**ERRSQ**		0.020	0.020	0.020	0.020	0.020
HYBRID		0.136	0.135	0.135	0.145	0.154	**HYBRID**		0.090	0.090	0.090	0.092	0.093
MPSD		3.695	3.682	3.682	3.810	3.936	**MPSD**		3.013	3.009	3.009	3.048	3.049
ARE		1.406	1.396	1.396	1.345	1.351	**ARE**		1.078	1.070	1.070	1.013	1.013
EABS		0.461	0.462	0.462	0.443	0.446	**EABS**		0.355	0.354	0.354	0.339	0.339
SNE		4.696	4.687	4.687	4.744	4.926	**SNE**		4.945	4.935	4.935	4.891	4.894
R^2:	0.989	χ^2: 0.008					R^2:	0.999	χ^2: 0.004				

Table 2. Non-linear isotherm parameters with error analysis of ZNa-Al sample

	LTFM	ERRSQ	HYBRID	MPSD	ARE	EABS		LTFM	ERRSQ	HYBRID	MPSD	ARE	EABS
Langmuir							***Freundlich***						
b (L mg^{-1})	65.852	61.314	62.984	62.984	60.980	60.990	K_f (mg g^{-1})	2.033	2.034	2.032	2.032	2.045	2.045
Q (mg g^{-1})	2.139	2.150	2.144	2.144	2.205	2.204	n	11.847	12.343	12.0763	12.076	11.762	11.791
ERRSQ		0.048	0.048	0.048	0.067	0.067	**ERRSQ**		0.0147	0.014	0.0148	0.016	0.016
HYBRID		0.502	0.499	0.499	0.705	0.704	**HYBRID**		0.147	0.145	0.145	0.159	0.159
MPSD		7.087	7.070	7.0708	8.397	8.393	**MPSD**		3.841	3.814	3.814	3.988	3.987
ARE		3.358	3.366	3.3663	2.903	2.903	**ARE**		2.029	2.020	2.020	1.925	1.925
EABS		0.465	0.471	0.471	0.398	0.398	**EABS**		0.283	0.285	0.285	0.274	0.274
SNE		**4.266**	4.279	4.279	4.706	4.704	**SNE**		4.767	**4.762**	**4.762**	4.910	4.905
R^2:	0.869	χ^2: 0.024					R^2:	0.969	χ^2: 0.007				
D-R							***Sips***						
q_m (mol·g^{-1})	4.2E-05	4.19E-05	4.19E-05	4.19E-05	4.19E-05	4.19E-05	q_m (mg g^{-1})		2.627	2.654	2.654	2.580	2.420
β	5.6E-10	5.53E-10	5.53E-10	5.53E-10	5.53E-10	5.53E-10	K_s (L mg^{-1})		3.718	3.535	3.535	3.983	6.323
ERRSQ		8.21E-11	1.48E-12	1.48E-12	1.48E-12	1.48E-12	m_s		0.308	0.300	0.300	0.313	0.403
HYBRID		1.08E-06	1.08E-06	0.000133	0.000133	0.000133	**ERRSQ**		0.004	0.004	0.004	0.004	0.006
MPSD		0.010	0.010	0.115	0.115	0.115	**HYBRID**		0.051	0.051	0.051	0.060	0.087
ARE		1.555	1.555	13.618	13.618	13.618	**MPSD**		2.277	2.272	2.272	2.466	2.958
EABS		2.95E-06	2.95E-06	2.21E-05	2.21E-05	2.21E-05	**ARE**		1.074	1.074	1.074	0.988	0.857
SNE		**1.345**	**0.363**	4.018	4.018	4.018	**EABS**		0.152	0.153	0.153	0.141	0.117
R^2:	0.990	χ^2: 5.4E-08					**SNE**		4.947	**3.986**	3.992	3.992	4.123
							R^2:	0.990	χ^2: 0.002				
R-P							***Toth***						
K_{RP} (L g^{-1})		347.319	362.286	362.275	346.457	346.309	q_m (mg g^{-1})		2.726	2.764	2.764	2.679	2.624
a_{RP} (L mg^{-1})		167.426	174.827	174.821	167.798	167.726	K		14.340	14.174	14.173	14.846	15.211
β_{RP}		0.942	0.940	0.940	0.944	0.944	M_t		0.244	0.234	0.234	0.248	0.265
ERRSQ		0.006	0.006	0.006	0.007	0.007	**ERRSQ**		0.004	0.004	0.004	0.005	0.005
HYBRID		0.075	0.075	0.075	0.087	0.087	**HYBRID**		0.054	0.053	0.053	0.063	0.062
MPSD		2.753	2.748	2.748	2.955	2.955	**MPSD**		2.324	2.319	2.319	2.515	2.503
ARE		1.286	1.291	1.291	1.223	1.223	**ARE**		1.094	1.095	1.095	1.025	1.003
EABS		0.1846	0.186	0.186	0.176	0.176	**EABS**		0.155	0.156	0.156	0.146	0.142
SNE		**4.646**	4.655	4.655	4.895	4.894	**SNE**		**4.647**	4.653	4.653	4.918	4.834
R^2:	0.985	χ^2: 0.005					R^2:	0.989	χ^2: 0.002				

Table 3. Non-linear isotherm parameters with error analysis of ZNa-AlFe sample

	LTFM	ERRSQ	HYBRID	MPSD	ARE	EABS		LTFM	ERRSQ	HYBRID	MPSD	ARE	EABS
Langmuir							***Freundlich***						
b (L mg^{-1})	97.526	75.698	81.141	81.141	100.601	97.782	K_f (mg g^{-1})	5.0664	5.068	5.066	5.066	5.118	5.121
Q (mg g^{-1})	5.110	5.251	5.191	5.191	5.295	5.345	n	10.458	10.409	10.42	10.421	10.584	10.568
ERRSQ		1.107	1.123	1.123	1.324	1.378	**ERRSQ**		0.049	0.049	0.049	0.067	0.069
HYBRID		4.972	4.907	4.907	6.078	6.399	**HYBRID**		0.213	0.213	0.213	0.2982	0.304
MPSD		22.298	22.153	22.153	24.653	25.297	**MPSD**		4.616	4.615	4.615	5.460	5.517
ARE		7.985	7.981	7.981	7.579	7.556	**ARE**		1.6166	1.620	1.620	1.488	1.481
EABS		2.510	2.548	2.548	2.408	2.373	**EABS**		0.528	0.530	0.530	0.479	0.476
SNE		**4.470**	4.480	4.480	4.805	4.903	**SNE**		**4.244**	4.250	4.250	4.768	4.812
R^2:	0.773	χ^2: 0.240					R^2:	0.989	χ^2: 0.026				
D-R							***Sips***						
q_m (mol·g^{-1})	0.00011	0.000111	0.000111	0.000111	0.000111	0.000111	q_m (mg g^{-1})		5.212	5.142	5.123	5.231	5.221
β	6.1E-10	6.3E-10	6.3E-10	6.3E-10	6.3E-10	6.3E-10	K_s (L mg^{-1})		2.4E-05	2.4E-05	2.47E-05	2.49E-05	2.49E-05
ERRSQ		2.02E-09	1.21E-11	2.3E-09	1.21E-11	1.21E-11	m_s		0.096	0.095	0.095	0.094	0.094
HYBRID		4.25E-06	4.25E-06	0.000774	0.000774	0.000774	**ERRSQ**		0.049	0.049	0.049	0.069	0.0695
MPSD		0.020	0.020	0.278	0.278	0.278	**HYBRID**		0.267	0.267	0.267	0.381	0.382
ARE		1.699	1.699	24.219	24.219	24.219	**MPSD**		5.169	5.168	5.168	6.180	6.181
EABS		6.9E-06	6.9E-06	9.05E-05	9.05E-05	9.05E-05	**ARE**		1.617	1.622	1.622	1.483	1.483
SNE		**1.226**	**0.231**	5.134	4.005	4.005	**EABS**		0.528	0.530	0.530	0.476	0.476
R^2:	0.998	χ^2: 2.1E-07					**SNE**		4.947	**4.221**	4.252	4.252	4.814
							R^2:	0.989	χ^2: 0.011				
R-P							***Toth***						
K_{RP} (L g^{-1})		1.9E+09	1.9E+09	1.9E+09	1.9E+09	1.9E+09	q_m (mg g^{-1})		5.122	5.212	5.286	5.231	5.114
a_{RP} (L mg^{-1})		3.8E+08	3.8E+08	3.8E+08	3.8E+08	3.8E+08	K		9.432	9.449	9.445	9.443	9.436
β_{RP}		0.903	0.904	0.904	0.904	0.905	M_t		0.002	0.002	0.002	0.002	0.002
ERRSQ		0.049	0.049	0.049	0.066	0.069	**ERRSQ**		0.049	0.049	0.049	0.065	0.065
HYBRID		0.267	0.267	0.267	0.363	0.381	**HYBRID**		0.268	0.268	0.268	0.353	0.352
MPSD		5.169	5.168	5.168	6.024	6.177	**MPSD**		5.182	5.181	5.181	5.944	5.936
ARE		1.617	1.622	1.622	1.488	1.483	**ARE**		1.619	1.624	1.625	1.495	1.496
EABS		0.528	0.530	0.530	0.478	0.476	**EABS**		0.528	0.530	0.53	0.479	0.479
SNE		**4.245**	4.251	4.251	4.707	4.812	**SNE**		**4.390**	4.397	4.398	4.829	4.823
R^2:	0.989	χ^2: 0.021					R^2:	0.989	χ^2: 0.024				

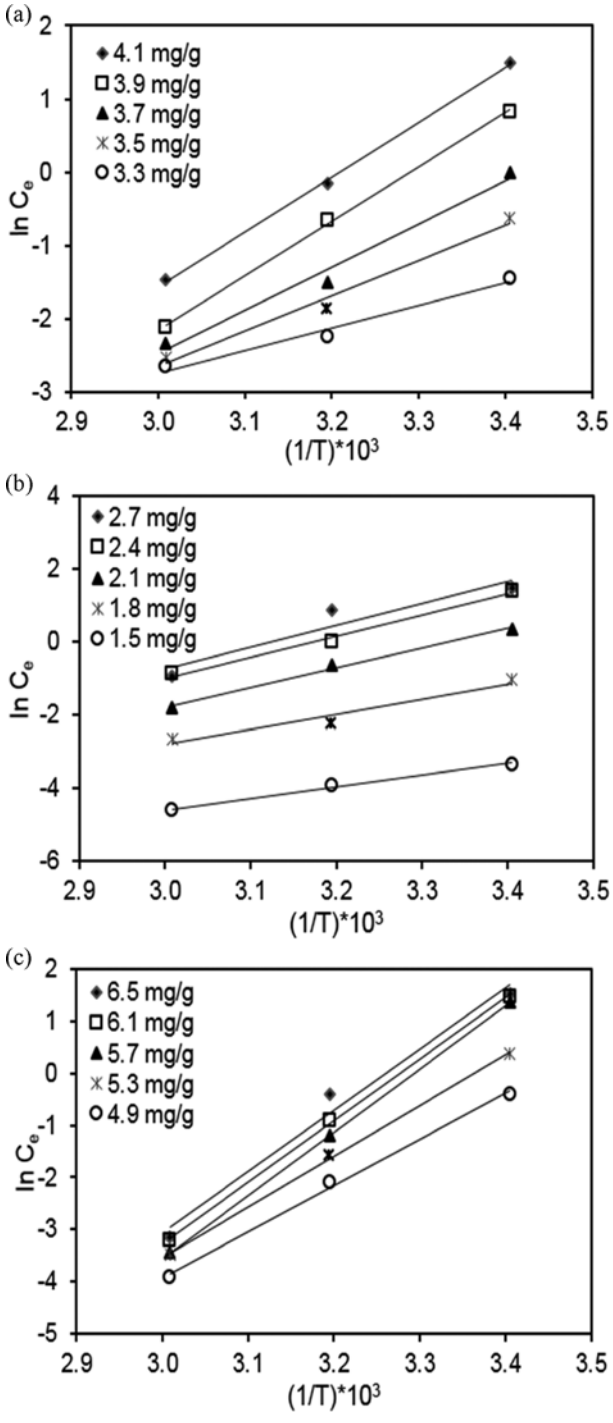

Fig. 6. Isosters of As(V) adsorption on samples at different surface loading (a) ZNa-Fe (b) ZNa-Al (c) ZNa-AlFe.

surface loading, indicating that the modified zeolites have an energetically homogeneous surface. Chowdhury et al. [39] stated that the dependence of ΔH_X on surface coverage could be due to the adsorbate-adsorbate interaction followed by adsorbate-adsorbent interaction. They indicated that the adsorbate-adsorbent interactions take place in high heats of adsorption as surface loading increases.

The ΔH_X values should be below 80 kJ mol^{-1} for physical adsorption, and for chemical adsorption they change between 80 and 400 kJ mol^{-1} [39]. The average ΔH_X values were calculated as 47.58

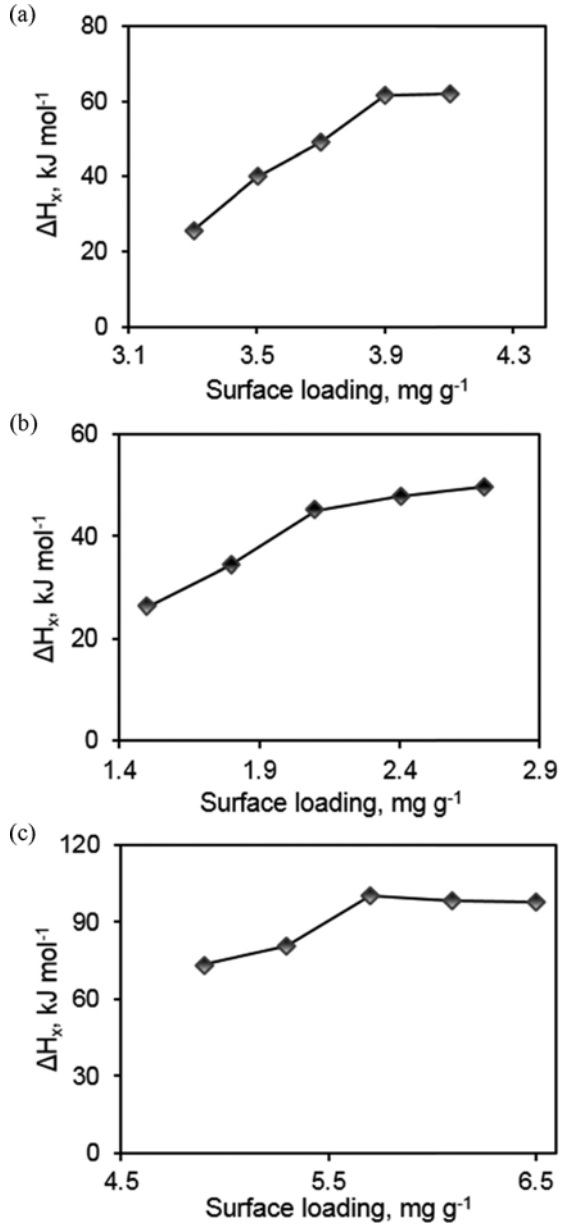

Fig. 7. Isosteric adsorption heats of (a) ZNa-Fe (b) ZNa-Al (c) ZNa-AlFe.

and 40.65 kJ mol^{-1} for ZNa-Fe and ZNa-Al, respectively. This fact indicates that the As(V) adsorption onto iron and aluminum modified zeolites was a physical process. However, the average ΔH_X value for ZNa-AlFe sample was found as 90.08 kJ mol^{-1}, which refers to chemical interaction between arsenate and binary metal oxides.

4. XPS Analysis and Adsorption Mechanism

The surface functional groups are helpful in order to explain the adsorption mechanisms. Therefore, the elemental composition and the changes in surface functional groups after arsenic adsorption were investigated using XPS analysis. In general, the major peaks for the Fe 2p, Al, O 1s, and As 3d spectrums were observed for the exhausted sorbents (Table 4). Also, the peaks at binding energy of 354±0.8 eV for Ca $2p_{3/2}$ appeared due to the composition of natural clinoptilolite for all samples. The O 1s spectra of iron and aluminum modified sorbents are illustrated in Fig. 8. For ZNa-Fe and

Table 4. XPS analysis results after As(V) adsorption

		Binding energy, (eV)	Peak area	FWHM, (eV)
ZNa-Fe				
	O 1s	529.138	297.799	1.378
		530.560	1605.503	2.191
		532.030	2804.746	2.469
	Fe 2p	711.230	2205.442	4.142
		723.588	575.002	6.388
	As 3d	44.419	51.326	1.702
		46.299	72.243	2.441
ZNa-Al				
	O 1s	529.571	310.933	1.423
		532.053	3918.970	2.332
		530.819	2178.416	2.012
	Al 2p	74.048	487.161	2.652
	Al 2s	102.369	331.401	2.289
	As 3d	45.203	67.326	1.986
ZNa-AlFe				
	O 1s	529.696	1902.096	2.204
		531.124	2510.661	1.777
		532.295	1372.142	2.052
	Fe 2p	710.383	1232.267	4.015
		715.856	492.553	6.500
		727.666	48.683	1.563
	Al 2p	73.456	275.229	2.107
	As 3d	42.415	36.939	1.622
		45.257	73.547	2.334

ZNa-AlFe sorbents, the peaks at binding energy of 529.138 and 529.696 eV can be assigned to Fe-O (lattice oxygen in magnetite or maghemite), respectively [39,41]. The peaks with binding energies of 530.560±1.7 eV can be attributed to the As-O bonds (As_2O_3, As_2O_5) on the arsenic-adsorbed samples [39,41]. The XPS spectra of ZNa-Fe sorbent obtained in the Fe 2p region are shown in Fig. 9. The Fe 2p region of the XPS spectrum often includes the peaks of Fe^0, Fe^{2+} and Fe^{3+} oxides. Barquist and Larsen [42] indicated that Fe_2O_3 (Fe^{3+}) and FeO (Fe^{2+}) have binding energies in the ranges of 711.1-719.8 eV and 709.9-715 eV, respectively. Moreover, the magnetite (Fe_3O_4) has a binding energy ranging from 710.5 to 711.2 V. The peaks located at 711.230 and 723.588 eV correspond to Fe $2p_{3/2}$ and Fe $2p_{1/2}$, respectively. The peak area of Fe $2p_{3/2}$ ($Area_{Fe2p3/2}$=2205.442) was found higher than that of Fe $2p_{1/2}$ ($Area_{Fe2p1/2}$=575.002), indicating that the Fe^{3+} oxide species are primarily present on the surface after adsorption. The presence of Fe^{3+} species could be attributed to the redox reactions that occurred during the uptake of arsenate, i.e., As(V) is reduced to As(III) while Fe^{2+} is oxidized to Fe^{3+} (Eqs. (18)-(19)).

$$Fe^{2+} \rightarrow Fe^{3+} \quad E_0 = -0.77 \text{ V};$$
$$H_3AsO_4 \rightarrow HAsO_2 \quad E_0 = +0.56 \text{ V} \tag{18}$$

$$Fe^{2+} + H_3AsO_4 \rightarrow Fe^{3+} + HAsO_2 + OH^- \tag{19}$$

Similar phenomenon was observed by Lim et al. [41]. They reported that the redox reactions might be followed by reduction of the surface bound As^V species to As^{III} via charge transport from Fe^{2+} species in the magnetite sorbent.

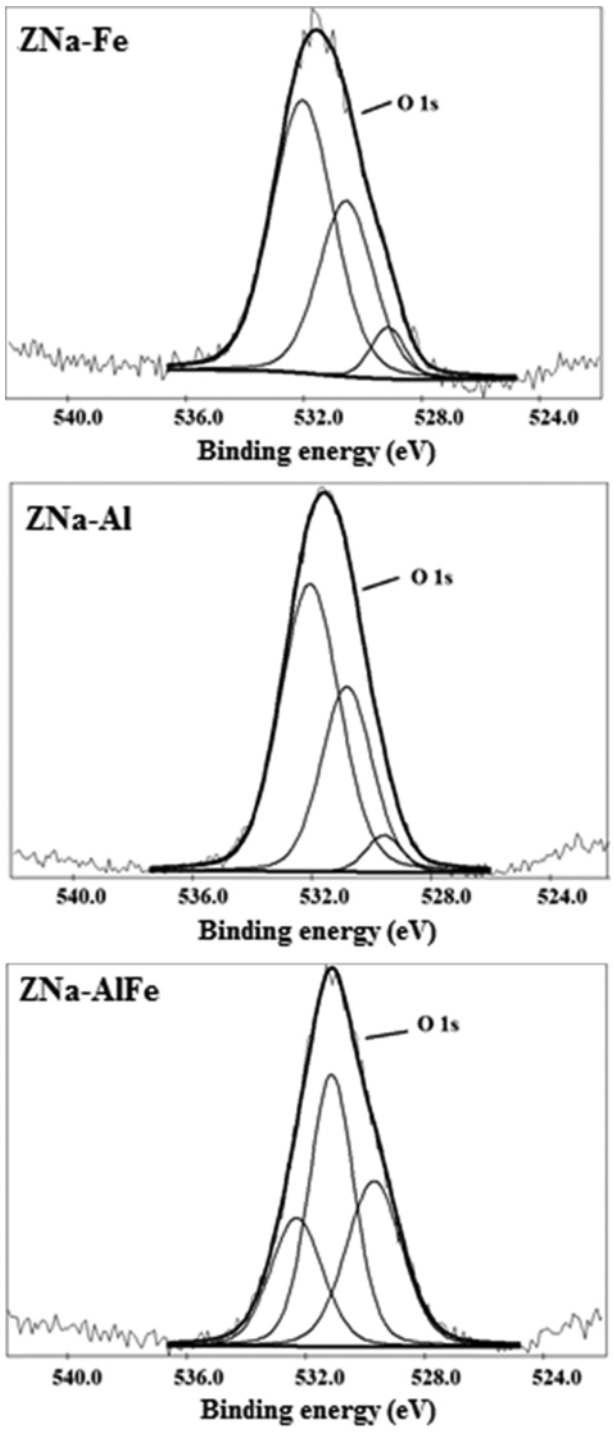

Fig. 8. O 1s spectrums of samples.

The metallic (Al^0) and trivalent aluminum (Al^{3+}) species have binding energies at ~73.2 eV and ~75 eV, respectively [43]. The Al 2s and Al 2p spectra of the ZNa-Al sample are shown in Fig. 10. The Al $2s_{1/2}$ peak at 102.369 eV and Al $2p_{1/2}$ peak at 74.048 eV are assigned to the AlOOH species on the aluminum coated zeolite.

As presented in Fig. 11, the binding energies of Fe 2p core were 710.383 and 715.856 eV, and the peak area values indicated that the dominant oxidation state of Fe was +III, for the ZNa-AlFe sam-

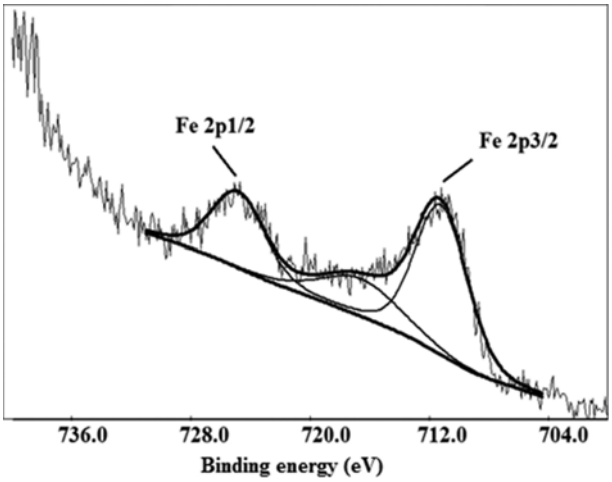

Fig. 9. Fe 2p spectrum of ZNa-Fe sample.

ple. The peak at the binding energy of 727.666 eV showed that Fe^{2+} species are also present in the zeolite structure. The peak area of Al $2p_{3/2}$ at the binding energy of 73.456 eV was calculated as 275.229, showing that the surface functional groups of the ZNa-AlFe sorbent mainly consist of iron (oxy) hydroxide species.

The As 3d core level of the arsenic loaded sorbent consisted of two individual component peaks originating from the different valences of the arsenic atom [41]. In Fig. 12, the XPS spectra of ZNa-Fe after As(V) adsorption showed two peaks; the binding energies of 44.419 and 46.299 eV should be attributed to As^{III}-O and As^{V}-O, respectively [39,44]. Similarly, the spectra of ZNa-AlFe included two peaks at 42.415 (As^{III}) and 45.257 eV (As^{V}). Therefore, it was demonstrated that there was little As^{III} oxidized into As^{V} in the adsorption system of iron oxide modified zeolites. Similar results about As^{III} formation on iron surfaces after treatment with As^{V} solution were reported by other researchers [39,44,45]. However, for the spectra of ZNa-Al sorbent, the binding energy related to As^{3+} species was not observed indicating that the adsorption process is followed by surface complexation reactions rather than redox interactions.

CONCLUSIONS

We examined the equilibrium As(V) adsorption onto mono- (Fe or Al) and binary (Fe/Al) oxides supported on natural zeolite. Nonlinear isotherm models were applied to the experimental data and error functions were used to determine the best fit isotherm. Among the two-parameter isotherms, the HYBRID and ERRSQ parameter sets produced the best fit to the D-R model by giving the lowest SNE values. The isosteric heats of adsorption (ΔH_X) values of ZNa-Fe and ZNa-Al indicated physical adsorption, while the value for ZNa-AlFe was found higher, which refers to chemical interactions.

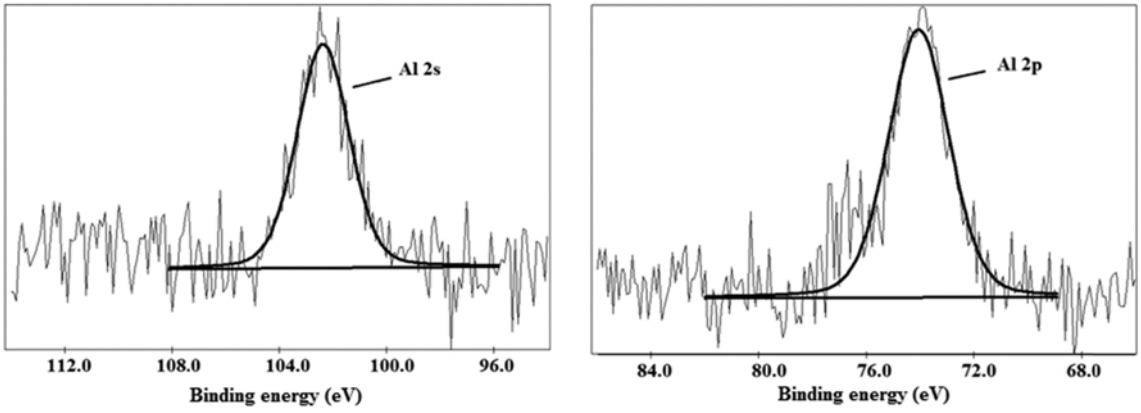

Fig. 10. Al 2s and Al 2p spectrums of ZNa-Al sample.

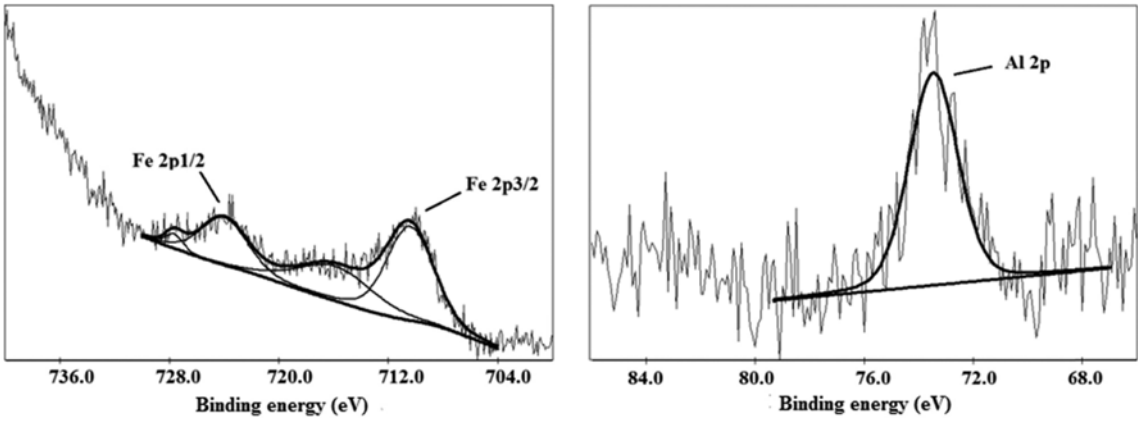

Fig. 11. Al 2p and Fe 2p spectrums of ZNa-AlFe sample.

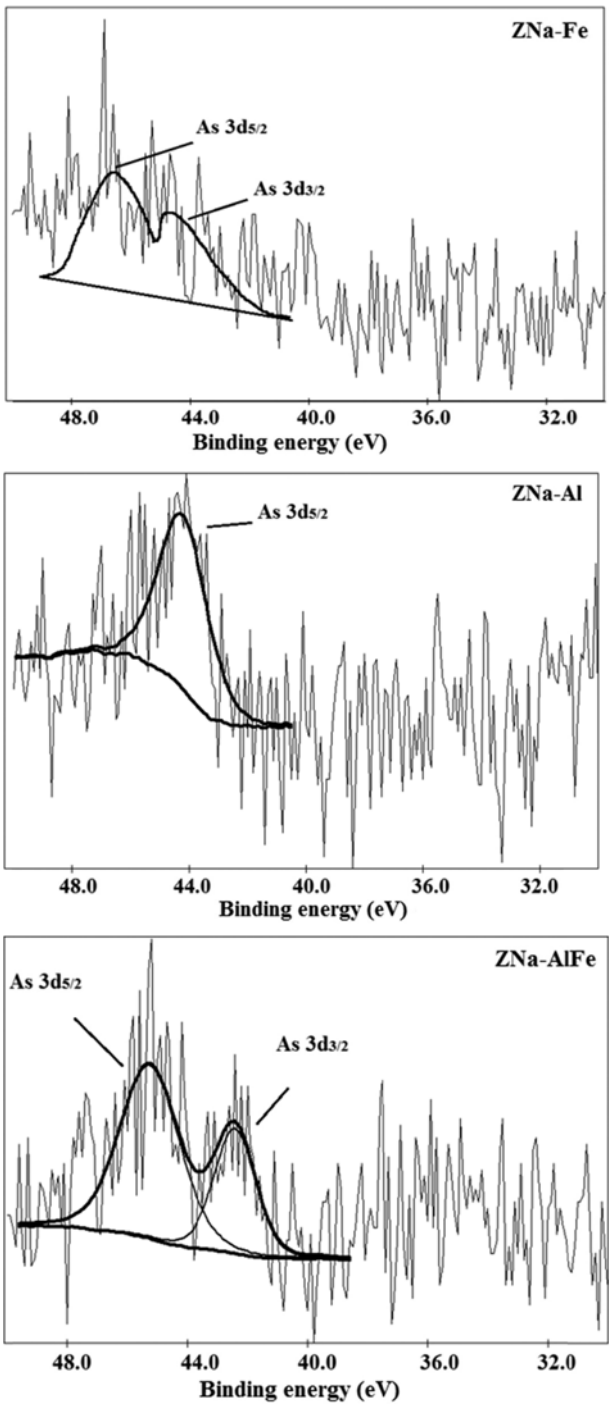

Fig. 12. As 3d spectrums of samples.

The XPS spectra of ZNa-Fe and ZNa-AlFe samples after As(V) adsorption showed two peaks related to As^{III}-O and As^{V}-O bonds, which demonstrated the fact that there was little As^{III} oxidized into As^{V} in the adsorption system of iron oxide modified zeolites.

REFERENCES

1. S. Bordoloi, S. K. Nath, S. Gogoi and R. K. Dutta, *J. Hazard. Mater.*, **260**, 618 (2013).
2. S. Lee, *Korean J. Chem. Eng.*, **27**, 110 (2010).
3. G. Liu, N. Liu, H. Zhang and L. Zhang, *Desalin. Water Treat.*, **21**, 96 (2010).
4. E. Bilgin Simsek, E. Özdemir and U. Beker, *Chem. Eng. J.*, **220**, 402 (2013).
5. M. J. Jiménez-Cedillo, M. T. Olguín, Ch. Fall and A. Colin, *Appl. Clay Sci.*, **54**, 206 (2011).
6. M. Šiljeg, Š. Cerjan Stefanovic, M. Mazajb, N. Novak Tušar, I. Arćon, J. Kovac, K. Margeta, V. Kaucic and N. Zabukovec Logar, *Micropor. Mesopor. Mater.*, **118**, 408 (2009).
7. B. Doušová, L. Fuitová, T. Grygar, V. Machovic, D. Koloušek, L. Herzogova and M. Lhotka, *J. Hazard. Mater.*, **165**, 134 (2009).
8. M. M. Dávila-Jiménez, M. P. Elizalde-González, J. Mattusch, P. Morgenstern, M. A. Pérez-Cruz, Y. Reyes-Ortega, R. Wennrich and H. Yee-Madeira, *J. Colloid Interface Sci.*, **322**, 527 (2008).
9. M. G. Macedo-Miranda and M. T. Olguin, *J. Incl. Phenom. Macro.*, **59**, 131 (2007).
10. Y. H. Xu, T. Nakajima and A. Ohki, *J. Hazard. Mater.*, **92**, 275 (2002).
11. B. Dousova, T. Grygar, A. Martaus, L. Fuitova, D. Kolousek and V. Machovic, *J. Colloid Interface Sci.*, **302**, 424 (2006).
12. A. Ramesh, H. Hasegawa, T. Maki and K. Ueda, *Sep. Purif. Technol.*, **56**, 90 (2007).
13. C. T. Yavuz, J. T. Mayo, W. W. Yu, A. Prakash, J. C. Falkner, S. Yean, L. Cong, H. J. Shipley, A. Kan, M. Tomson, D. Natelson and V. L. Colvin, *Science*, **314**, 964 (2006).
14. D. E. Giles, M. Mohapatra, T. M. Issa, S. Anand and P. Singh, *J. Environ. Manage.*, **92**, 3011 (2011).
15. Y. Masue, R. H. Loeppert and T. A. Kramer, *Environ. Sci. Technol.*, **41**, 837 (2007).
16. Y. Zhang, M. Yang and X. M. Don, *Environ. Sci. Technol.*, **39**, 7246 (2005).
17. H. J. Hong, W. Farooq, J. S. Yang and J. W. Yang, *Sep. Sci. Technol.*, **45**, 1975 (2010).
18. J. Silva, J. W. V. Mello, M. Gasparon, W. A. P. Abrahao, V. S. T. Ciminelli and T. Jong, *Water Res.*, **44**, 5684 (2010).
19. A. Dabrowski, *Adv. Colloid Interface Sci.*, **93**, 135 (2001).
20. K. Y. Foo and B. H. Hameed, *Chem. Eng. J.*, **156**, 2 (2010).
21. D. M. Ruthven, *Principles of adsorption and adsorption processes*, Wiley, New York (1984).
22. I. Langmuir, *J. Am. Chem. Soc.*, **40**, 1361 (1918).
23. T. W. Webber and R. K. Chakkravorti, *AIChE J.*, **20**, 228 (1974).
24. F. Haghseresht and G. Lu, *Energy Fuels*, **12**, 1100 (1998).
25. M. K. Ghosh, G. E. Jai Poinern, T. B. Issa and P. Singh, *Korean J. Chem. Eng.*, **29**, 99 (2012).
26. J. Toth, *Adsorption theory modeling and analysis*, Marcel Dekker, New York (2002).
27. M. M. Dubinin, *Chem. Rev.*, **60**, 235 (1960).
28. O. Redlich and D. L. Peterson, *J. Phys. Chem.*, **63**, 1024 (1959).
29. J. Toth, *J. Colloid Interface Sci.*, **225**, 378 (2000).
30. T. S. Anirudhan and P. G. Radhakrishnan, *Desalination*, **249**, 1298 (2009).
31. R. T. Yang, *Adsorbents: Fundamentals and applications*, Wiley, New Jersey (2003).
32. A. B. Pérez-Marín, V. Meseguer Zapata, J. F. Ortuno, M. Aguilar, J. Sáez and M. Llorens, *J. Hazard. Mater.*, **B139**, 122 (2007).
33. M. I. El-Khaiary and G. F. Malash, *Hydrometallurgy*, **105**, 314 (2011).

34. S. J. Allen, G. Mckay and J. F. Porter, *J. Colloid Interface Sci.*, **280**, 322 (2004).
35. J. F. Porter, G. McKay and K. H. Choy, *Chem. Eng. Sci.*, **54**, 5863 (1999).
36. F. Gimbert, N. Morin-Crini, F. Renault, P. M. Badot and G. Crini, *J. Hazard. Mater.*, **157**, 34 (2008).
37. E. Demirbas, M. Kobya and A. E. S. Konukman, *J. Hazard. Mater.*, **154**, 787 (2008).
38. S. M. G. Demneh, B. Nasernejad and H. Modarres, *Colloids Surf., B*, **88**, 108 (2011).
39. S. R. Chowdhury, E. K. Yanful and A. R. Pratt, *Environ. Earth Sci.*, **64**, 411 (2011).
40. S. Sircar, R. Mohr, C. Ristic and M. B. Rao, *J. Phys. Chem. B*, **103**, 6539 (1999).
41. S. H. Lim, Y. U. Zheng and J. P. Chen, *Langmuir*, **25**(9), 4973 (2009).
42. K. Barquist and S. C. Larsen, *Micropor. Mesopor. Mater.*, **130**, 197 (2010).
43. E. Paparazzo, *Vacuum*, **62**, 47 (2001).
44. S. Bang, M. D. Johnson, G. P. Korfiatis and X. Meng, *Water Res.*, **39**, 763 (2005).
45. G. S. Zhang, J. Qu, H. Liu, R. Liu and R. Wu, *Water Res.*, **41**, 1921 (2007).